Proceedings of IMECE2005
2005 ASME International Mechanical Engineering Congress and Exposition
November 5-11, 2005, Orlando, Florida USA

IMECE2005-82591

# Three-Dimensional Simulation of Multiple Line Laser Sintering of a Two-Component Metal Powder Layer on Top of Sintered Layers

Tiebing Chen and Yuwen Zhang
Department of Mechanical and Aerospace Engineering
University of Missouri-Columbia
Columbia, MO 65211

## ABSTRACT

Multiple line laser scan sintering of a two-component metal powder layer on top of the sintered layers with a moving circular Gaussian laser beam is modeled numerically. The overlap between the adjacent scan lines to achieve enhanced bonding is taken into account. The binding between the newly sintered layer and existing sintered layers underneath through melting is also considered. The governing equation is formulated by a temperature-transforming model with partial shrinkage induced by melting considered. The liquid flow of the molten low melting point metal powders, which is driven by capillary and gravity forces, is formulated by Darcy's law. The effects of the dominant processing parameters, including the moving laser beam intensity, scanning speed and number of the existing sintered layers underneath, on the shape of the heat affected zone (HAZ) are investigated. A parametric study is performed and the best combination of the processing parameters is recommended.

## INTRODUCTION

Selective Laser Sintering (SLS) is one of the few rapid prototyping processes that possess the capability of producing three-dimensional, structurally sound, and fully functional parts directly from polymers, ceramics and metals without the use of any intermediate binders. It is a layered manufacturing method that can create functional parts by fusing powdered materials with a directed laser (generally $CO_2$ or YAG) beam [1]. Before laser scanning, a thin (100 - 250 $\mu m$ thick) powder layer is spread on the building substrate by a roller. The laser beam then selectively sinters or melts the powders, and then bonds powders into two-dimensional slices. After laser scanning, a fresh powder layer is spread and the scanning process is repeated until a 3-D part is fabricated. A brief review of the basic principles of SLS machine operation, and materials issues affecting direct SLS of metals, and the resultant properties and microstructures of the parts are discussed by Agarwala *et al.* [2]. An overview of the latest progress on selective laser sintering (SLS) works as reported in various journals and proceedings is presented by Kumar [3].

Melting and resolidification are the mechanisms to bond metal powder particles to form a layer and to bond different layers together to form a functional part. Fundamentals of melting and solidification have been investigated extensively and detailed reviews are available in the literatures [4, 5]. The distinctive feature of laser-induced melting of the metal powders in the SLS process is that it is always accompanied by the shrinkage due to the significant density change. When a single-component metal powder system is used in SLS process, what left behind after laser scanning is a series of sphere with diameter comparable to the size of the laser beam; this is referred to as balling phenomenon [6]. To avoid this balling phenomenon, the powder mixture that is composed of two types of powders that possess significantly different melting points was suggested by Bunnell [7] and Manzur *et al.* [8]. In case of two-component sintering, a molten liquid that is formed by melting the lower melting point powders infiltrates into the voids between the higher melting point solid powders and binds them together. Meanwhile, the solid particles moves downward because of the high melting point powder alone cannot sustain the powder bed structure. It should be noted that only the low-melting-point powder melts and resolidifies and the high melting point powders remain solid throughout the process. Pak and Plumb [9] presented a one-dimensional thermal model for melting of the two-component powder bed, in which the liquid motion driving by capillary and

 

gravitational forces is considered but the shrinkage was neglected. Zhang and Faghri [10] analytically solved one-dimensional melting of a semi-infinite two-component metal powder bed heated by a constant heat flux. Chen and Zhang [11] obtained the analytical solution of one-dimensional melting of the two-component metal powder bed with finite thickness subjected to a constant heat flux. Zhang and Faghri [12] simulated two-dimensional melting and resolidification of a subcooled two-component metal powder bed subject to a moving Gaussian heat source; shrinkage was accounted for but the liquid flow of the low melting point metal is neglected. A two-dimensional model of multiple-layer SLS of a subcooled two-component metal powder layer with a moving Gaussian laser beam and adiabatic boundary condition at the bottom presented in by Chen and Zhang [13]. A three-dimensional finite element simulation for temperature evolution in the SLS process was conducted by Kolossov *et al.* [14], who considered the nonlinear behavior of thermal conductivity and of specific heat due to temperature changes and phase transformations. A three-dimensional thermal model of SLS of two-component metal powder bed was presented by Zhang *et al.* [15], who considered the effects of the solid particle velocity induced by shrinkage of the powder bed and the liquid flow driven by capillary and gravitational forces. The thickness of the powder bed used in Ref. [15] was very large, which approximated the sintering process of the first layer with the complete shrinkage. Melting and resolidification of a 3-D metal powder layer with a finite thickness heated by a moving Gaussian laser beam was investigated numerically by Chen and Zhang [16].

The porosity, $\varepsilon$, defined as volume fraction of void that can be occupied by either gas or liquid, is equal to $\varphi_{g,s}$ in the loose powder and it becomes $\varphi_\ell + \varphi_{g,\ell}$ after melting. If the volume of the gas being driven out from the powder bed is equal to the volume of the liquid generated during melting, the porosity of the powder bed before and after melting will be the same, i.e., $\varepsilon = \varphi_{g,s} = \varphi_s + \varphi_{g,\ell}$; this is referred to as constant porosity model [9]. If the volume fractions of high and low melting point powders before sintering satisfy $\varphi_s/(\varphi_H + \varphi_s) = \varphi_{g,s}$, the powder bed can be fully densified ($\varphi_{g,\ell} = 0$) under constant porosity model [15, 16]. On the other extreme, if there is no shrinkage, one would expect that $\varphi_{g,\ell} = \varphi_{g,s}$ and the porosity, $\varepsilon$, increases since $\varphi_\ell$ increases during melting. In reality, the volume fraction of gas in the HAZ may not be zero because the life span of the liquid is not long enough to allow all gas escape from the powder bed [15]. Therefore, the rate of the shrinkage in the SLS process may be somewhere between the complete shrinkage and no shrinkage. A partial shrinkage model for SLS of the two-component metal powders was developed and the effects of the volume fraction of the gas in the HAZ on the shape and size of HAZ were investigated by the authors [17]. Three-dimensional sintering process of the two-component metal powders for a single-line scanning of a loose powder layer on top of the existing sintered metal layers was investigated by Chen and Zhang [18], and partial shrinkage model in Ref. [17] was employed.

In this paper, a three-dimensional multiple line laser scanning sintering process of a two-component metal powder layer on the top of multiple existing sintered layers will be investigated. To obtain the sound metallic bonding between sintered layers, the overlaps between vertically deposited layers as well as lines at horizontal neighbors are considered. The effects of the volume fraction of the gas in the HAZ, laser scanning velocity and the number of the existing sintered layers on the shape of the HAZ will be discussed.

## NOMENCLATURE

| | |
|---|---|
| $Bi$ | Biot number, $hR/k_H$ |
| $Bo$ | Bond Number, $\rho_\ell g R d_p/\gamma_m^0$ |
| $C$ | dimensionless heat capacity, $C^0/C_H^0$ |
| $C^0$ | heat capacity, $\rho c_p$, $(J/m^3\text{-}K)$ |
| $c_p$ | specific heat, ($J/kg\text{-}K$) |
| $d_p$ | diameter of the powder particle (m) |
| $g$ | gravitational acceleration ($m/s^2$) |
| $h$ | convective heat transfer coefficient, ($W/m^2\text{-}K$) |
| $h_{s\ell}$ | latent heat of melting or solidification, $J/kg$ |
| **i** | unit vector in x direction |
| $I_0$ | laser intensity at the center of the laser beam, ($W/m^2$) |
| **j** | unit vector in y direction |
| $k$ | thermal conductivity, ($W/mK$) |
| **k** | unit vector in z direction |
| $K$ | permeability, or dimensionless thermal conductivity, $k/k_H$ |
| $K_{r\ell}$ | relative permeability |
| $Ma$ | Marangoni number, $\gamma_m^0 d_p/(\alpha_H \mu)$ |
| N | number of existing sintered layers |
| $N_i$ | dimensionless laser intensity, $\alpha_a I_0 R/[k_H(T_m^0 - T_i^0)]$ |
| $N_R$ | radiation number, $\varepsilon_e \sigma (T_m^0 - T_i^0)^3 R/k_H$ |
| $N_t$ | temperature ratio for radiation, $T_m^0/(T_m^0 - T_i^0)$ |
| $p$ | pressure ($N/m^2$) |
| $P_c$ | dimensionless capillary pressure, $p_c/(\gamma_m^0\sqrt{\varepsilon/K})$ |
| $R$ | radius of the moving laser beam at 1/e ($m$) |
| $s$ | solid-liquid interface location ($m$) |
| $s_0$ | location of surface ($m$) |
| $s_{st}$ | sintered depth ($m$) |
| $Sc$ | subcooling parameter, $C_L^0(T_m^0 - T_i^0)/(\rho_L h_{s\ell})$ |

$T$ dimensionless temperature, $(T^0 - T_m^0)/(T_m^0 - T_i^0)$
$t$ false time (s)
$T^0$ temperature ( $K$ )
$u_b$ laser beam moving velocity ( $m/s$ )
$U_b$ dimensionless heat source moving velocity, $u_b R/\alpha_H$
$\mathbf{v}$ velocity vector, $u\mathbf{i} + v\mathbf{j} + w\mathbf{k}$
$\mathbf{V}$ dimensionless velocity vector, $\mathbf{v}R/\alpha_H$
$\forall$ volume ( $m^3$ )
$x, y, z$ coordinate, (m)
$X, Y, Z$ dimensionless moving horizontal coordinate, $(x, y, z)/R$

**Greek symbol**

$\alpha$ thermal diffusivity ( $m^2\ s^{-1}$ )
$\alpha_a$ absorbtivity
$\gamma^0$ surface tension, $(N/m^2)$
$\gamma$ dimensionless surface tension, $\gamma^0/\gamma_m^0$
$\gamma_m^0$ surface tension of the low melting point metal at melting point, $(N/m^2)$
$\delta$ powder layer thickness, (m)
$\Delta$ dimensionless powder layer thickness, $\delta/R$
$\Delta T^0$ one-half of phase-change temperature range ( $K$ )
$\Delta T$ one-half of dimensionless phase change temperature range
$\varepsilon$ porosity for unsintered powder, $(\forall_g + \forall_\ell)/(\forall_g + \forall_\ell + \forall_s + \forall_H)$
$\varepsilon_e$ emissivity of surface
$\eta$ dimensionless location of the solid-liquid interface, $s/R$
$\eta_0$ dimensionless location of the surface, $s_0/R$
$\eta_{st}$ dimensionless sintered depth, $s_{st}/R$
$\rho$ density ( $kg/m^3$ )
$\sigma$ Stefan-Boltzmann constant, $5.67\times10^{-8}\ W/(m^2 \cdot K^4)$
$\tau$ dimensionless false time, $\alpha_H t/R^2$
$\varphi$ volume fraction
$\dot{\Phi}_L$ dimensionless volume production rate of the liquid
$\psi$ saturation, $\varphi_l/\varepsilon$
$\nabla$ dimensionless gradient operator, $\mathbf{i}(\partial/\partial X) + \mathbf{j}(\partial/\partial Y) + \mathbf{k}(\partial/\partial Z)$

**Subscripts**

$c$ capillary
$g$ gas(es)
$eff$ effective
$H$ high melting point powder
$i$ initial
$\ell$ liquid or sintered region
$L$ low melting point powder
$m$ melting point
$p$ existing sintered region
$s$ solid

## Physical model

During the SLS process, the position of the laser beam will be reset and begin to start another scan along the *x*-direction. The scan spacing determines the overlap between the adjacent lines. Values of scan spacing are small, typically 0.5, 0.25 or 0.125 of the laser beam diameter [19]. The value of overlap between lines is assumed to be 0.5 in this paper in order to get optimum bonding which aids densification. After the completion of the sintering process on *x*-*y* plane, the sintered layer is lowered and a fresh layer of powders is spreads into the build zone in order to repeat the process. Bonding also occurs between layers as the new layer is sintered, i.e., the overlap between newly sintered layers and existed sintered layers below is considered. The sintering depth will pierce into the previously sintered layers below so that the newly sintered layer can be bound the existing layer to form an integrated resolidified region. The overlap between layers is defined as the ratio of the width of the liquid pool at the bottom surface of the fresh layer and that of the liquid pool at the top surface; it is taken as 50% in this study.

The physical model of the multiple line scanning problem is shown in Fig. 1. It is assumed that the laser beam diameter is much smaller than the horizontal sizes of the workpiece to be built. The first layer sits on top of the existing sintered layers. The half of the first layer ($y$<0) is sintered while another half ($y$>0) is still loose powder. Laser sintering takes place at the center of the laser beam that coincides with the origin of the coordinate system. Therefore, the top surface of the physical domain before the sintering process is not a flat surface. The configuration of previously scanned line at neighbor needs to be considered. The shape of the previously sintered region can be estimated by the regression of the HAZ shape in single scan line model with the same porosity and number of existed sintered layers below. Therefore, the physical domain will have different shapes of the top surface for different rate of shrinkage. The initial top surface profiles of the physical domain, i.e., $S_0$ and $S$, are regressed approximately from the simulation results in Ref. [18] for all cases. In this paper, the different shrinkage rate due to the different volume fraction of gas in the liquid phase, $\varphi_{g,\ell}$, will be considered in the physical problem.

The energy equation, formulated by a temperature transforming model [20], is

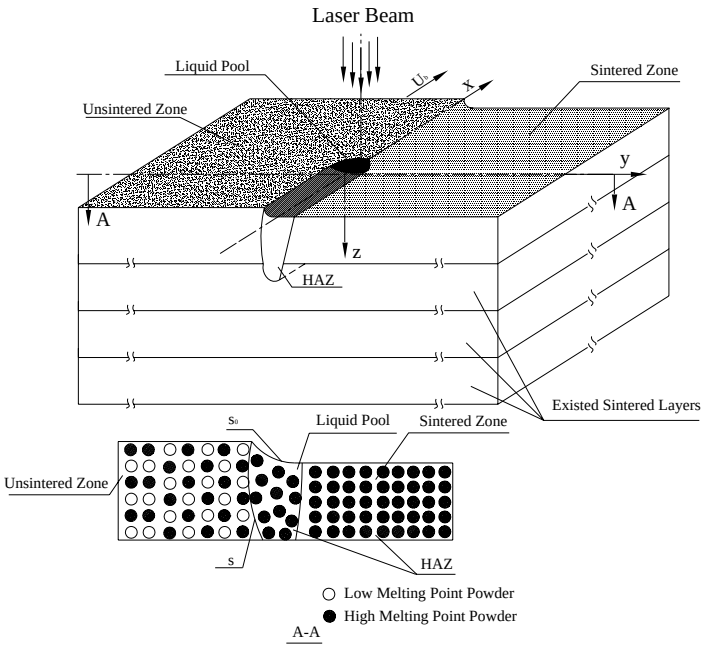


Fig. 1 Physical Model

$$\nabla\cdot(\varphi_\ell \mathbf{V}_\ell C_L T)-U_b\frac{\partial}{\partial X}[(\varphi_H+\varphi_s C_L)T]+W_s\frac{\partial}{\partial Z}[(\varphi_H+\varphi_s C_L)T]$$
$$=\nabla\cdot(K\nabla T)-\left\{\frac{\partial}{\partial\tau}[(\varphi_\ell+\varphi_s)S]+\nabla\cdot(\varphi_\ell\mathbf{V}_\ell S)+W_s\frac{\partial}{\partial Z}(\varphi_s S)-U\frac{\partial}{\partial X}[(\varphi_\ell+\varphi_s)S\right\} \quad (1)$$

where $W_s$ is the shrinkage velocity

$$W_s=\begin{cases}\dfrac{\varphi_{si}}{1-\varepsilon}\left(\dfrac{\partial\eta_{st}}{\partial\tau}-U\dfrac{\partial\eta_{st}}{\partial X}\right) & Z\le\eta_{st}\le\Delta\\ 0 & Z>\eta_{st}\end{cases} \quad (2)$$

which has a non-zero value in the liquid pool but equals zero in the resolidified region and the loose powder.

The heat capacity, C, source term, S, and thermal conductivity, $K$, respectively, are

$$C=(\varphi_s+\varphi_\ell)C_L+\varphi_H \quad (3)$$

$$C_L=\begin{cases}C_L & T<-\Delta T\\ C_L\left(1+\dfrac{1}{2\,Sc\,\Delta T}\right) & -\Delta T<T<\Delta T\\ C_L & T>\Delta T\end{cases} \quad (4)$$

$$S=\begin{cases}0 & T<-\Delta T\\ \dfrac{C_L}{2\,Sc} & -\Delta T<T<\Delta T\\ \dfrac{C_L}{Sc} & T>\Delta T\end{cases} \quad (5)$$

$$K=\begin{cases}K_{eff} & T<-\Delta T\\ K_{eff}+\dfrac{K_\ell-K_{eff}}{2\Delta T}(T+\Delta T) & -\Delta T<T<\Delta T\\ K_\ell & T>\Delta T \text{ or in HAZ}\end{cases} \quad (6)$$

The dimensionless velocities of the liquid phase, $\mathbf{V}_\ell$, can be obtained by Darcy's law [16]

$$\mathbf{V}_\ell-(-U_b\mathbf{i}+W_s\mathbf{k})=\frac{\varepsilon\,Ma\,\psi_e^3}{\sqrt{180}(1-\varepsilon)^2\psi}\nabla P_c+\frac{\varepsilon^2\,Ma\,Bo\,\psi_e^3}{180(1-\varepsilon)^2\psi}\mathbf{k} \quad (7)$$

where

$$Ma=\frac{\gamma_m^0\,d_p}{\alpha_H\mu},\quad Bo=\frac{\rho_\ell g\,R\,d_p}{\gamma_m^0} \quad (8)$$

The dimensionless capillary pressure, $P_c$, in eq. (7) can be calculate by [21],

$$P_c=1.417(1-\psi_e)-2.12(1-\psi_e)^2+1.263(1-\psi_e)^3 \quad (9)$$

where the normalized saturation, $\psi_e$, in eq. (9) is obtained by

$$\psi_e=\begin{cases}\dfrac{\psi-\psi_{ir}}{1-\psi_{ir}} & \psi>\psi_{ir}\\ 0 & \psi\le\psi_{ir}\end{cases} \quad (10)$$

and $\psi_{i,r}$ is the irreducible saturation.

The volume fraction of the liquid phase of the low melting point powders, $\varphi_\ell$, can the obtained from dimensionless continuity equation of the liquid in the moving coordinate system

$$\frac{\partial\varphi_\ell}{\partial\tau}-U_b\frac{\partial\varphi_\ell}{\partial X}+\nabla\cdot(\varphi_\ell\mathbf{V}_\ell)=\dot{\Phi}_L \quad (11)$$

The continuity equations for the solid phase of the low melting point powder and high melting point powder by assuming shrinkage occurs in the z- direction only are

$$\frac{\partial \varphi_s}{\partial \tau} - U_b \frac{\partial \varphi_s}{\partial X} + \frac{\partial (\varphi_s w_s)}{\partial Z} = -\dot{\Phi}_L \tag{12}$$

$$\frac{\partial \varphi_H}{\partial \tau} - U_b \frac{\partial \varphi_H}{\partial X} + \frac{\partial (\varphi_H w_s)}{\partial Z} = 0 \tag{13}$$

and the following relationship is valid in all regions

$$\varepsilon + \varphi_s + \varphi_H = 1 \tag{14}$$

The volume production rate, $\dot{\Phi}_L$, can be obtained by combining eqs. (12) – (14), i.e.,

$$\dot{\Phi}_L = -\frac{\partial (1-\varepsilon)}{\partial \tau} + U_b \frac{\partial (1-\varepsilon)}{\partial X} - \frac{\partial}{\partial Z}\left[(1-\varepsilon) W_s\right] \tag{15}$$

where the porosity, $\varepsilon$, is not constant during the sintering process under the partial shrinkage model since the porosity, $\varepsilon$, is defined as volume fraction of void that can be occupied by either gas or liquid. The value of the porosity depends on the volume fraction of the gas in the loose powders or HAZ. The location of liquid surface is related to the sintered depth by

$$\eta_0(X,Y) = \begin{cases} \dfrac{1-\varepsilon_\ell - \varphi_{H,i}}{1-\varepsilon_\ell} \eta_{st}(X,Y) & \eta_{st} < \Delta_s \\ \dfrac{1-\varepsilon_\ell - \varphi_{H,i}}{1-\varepsilon_\ell} \Delta_s & \eta_{st} \geq \Delta_s \end{cases} \tag{16}$$

The corresponding boundary and initial equations are

$$-K\frac{\partial T}{\partial Z} = N_i \exp(-X^2 - Y^2) - N_R[(T+N_t)^4 - (T_\infty + N_t)^4] - Bi(T - T_\infty) \quad Z = \eta_0(X) \tag{17}$$

$$\frac{\partial T}{\partial Z} = 0 \ , \ Z = \Delta_s + N\Delta_\ell \tag{18}$$

$$\frac{\partial T}{\partial X} = 0 \ , \ |X| \to \infty \tag{19}$$

$$\frac{\partial T}{\partial Y} = 0 \ , |Y| \to \infty \tag{20}$$

## Numerical solutions

The optimum combinations of dimensionless laser beam intensity and scanning velocity are sought to obtain the expected sintering depth and the overlaps between the newly sintered layers and the existing sintered layers. The energy equation is solved by the false transient method in the moving coordinate system. The converged steady-state solution is obtained when the temperature distribution does not change with the false time. For any given laser scanning velocity, computation is performed with different laser intensities beginning with a lower intensity, at which the desired sintering depth is not reached. The laser intensity will then be gradually increased until the required sintering depth and 50% overlap between HAZ and existing sintered layers underneath are obtained. The false transient time step in the paper is 0.12 and the grids number are $92 \times 72 \times 22$ ($X \times Y \times Z$). The grids in the $X$- and $Y$-directions are non-uniform but uniform in the $Z$-direction. A block-off technique [22] is used to transfer the irregular physical domain into the regular computational domain in order to simplify the numerical calculation. The irregular shape of the physical domain is caused by the possible movement of the top liquid surface due to the shrinkage and possible irregular initial shape of the physical domain by considering multiple laser scan lines. The thermal conductivity in the empty space created by the shrinkage is zero. Iterations are needed due to the coupled procedures to obtain solutions of velocities of the liquid phase of the low melting point powder and $\varphi_\ell$.

## Results and discussions

Effects of the volume fraction of the gas in the Heat Affected Zone (HAZ) on the shape of HAZ are investigated. The combined optimal scanning velocities and the intensities of the laser beam that can yield the required sintering depth and overlaps are obtained. The 3-D shapes of the HAZ with different volume fraction of the gas in HAZ, $\varphi_{g,\ell}$, with one existing sintered layer underneath are shown in Fig. 2. The shrinkage is smaller when the volume fraction of gas in the liquid pool increases and there is no shrinkage when $\varphi_{g,\ell}$ is up to $\varphi_{g,s}$. The optimal laser beam intensity increases with increasing $\varphi_{g,\ell}$ in order to obtain the same sintering depth and overlap because a higher $\varphi_{g,\ell}$ causes the smaller shrinkage and thicker existing sintered layers underneath. Part of the initially overlapped region, which was the resolidified region after previous scanning, re-melts again. Therefore, the neighbored scan lines can have a solid bond after the liquid metal is resolidified again when the laser beam moves away. In addition, the higher magnitude of the laser power is needed since the thermal conductivity of the existed sintered layers is much higher than that of the loose powder layer. The HAZ becomes more porous with increasing volume fraction of the gas in HAZ, which in turn will cause the weak density of the sintered part. Figure 3 shows the surface temperature distribution of the powder layer at the quasi-steady-state during the sintering process. The surface temperature of the overlap region is higher than that of the loose powders.

Table 1 Sintering parameters applied in numerical simulations

| | | | |
|---|---|---|---|
| Bi | $2.94\times10^{-4}$ | $N_R$ | $4.2\times10^{-4}$ |
| Bo | $5.3\times10^{-3}$ | $Sc$ | 1.38 |
| $C_L$ | 1.07 | $T_\infty$ | -1.0 |
| $K_g$ | $5.38\times10^{-4}$ | $\varphi_{gs}$ | 0.42 |
| $K_L$ | 0.2 | $\varphi_{g,\ell}$ | 0.0, 0.2, 0.42 |
| Ma | 1042.0 | $\psi_{ir}$ | 0.08 |
| $N_t$ | $1.19\times10^{-3}$ | $\Delta T$ | 0.001 |
| $N$ | 1, 3 | | |

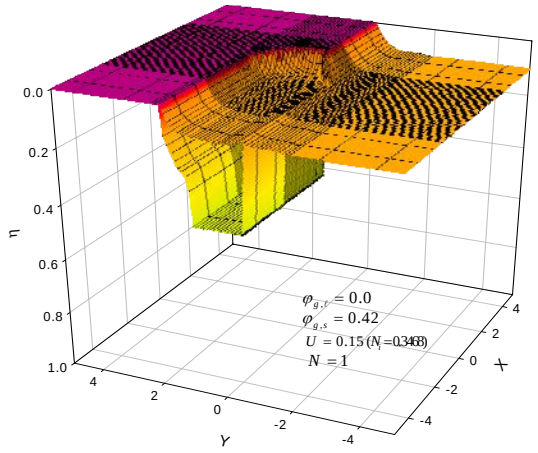


(a)

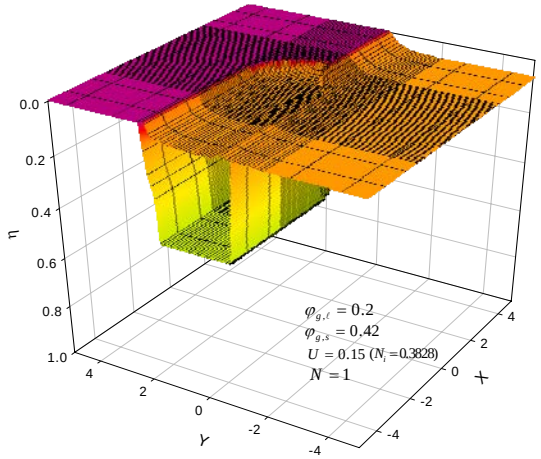


(b)

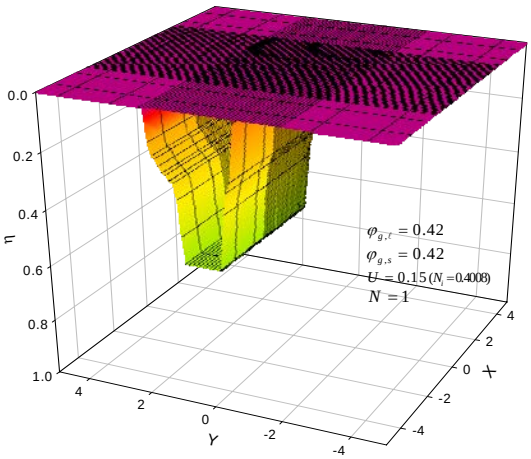


(c)

Fig. 2 Three-dimensional shape of the HAZ ($\Delta_s = 0.25$, $U = 0.1$, $N = 1$)

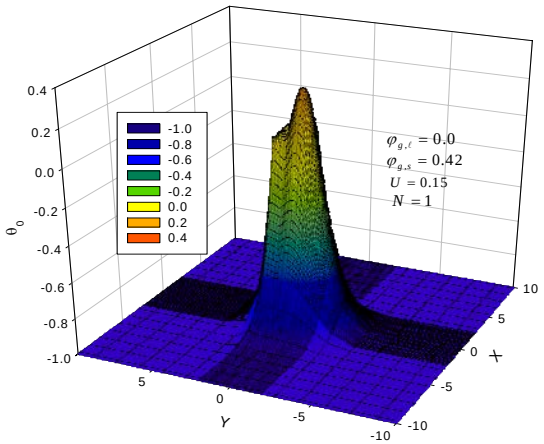


Fig. 3 The temperature distribution at the surface of the powder layer ($\Delta_s = 0.25$, $U = 0.1$, $\varphi_{g\ell} = 0.2$)

Figures 4-6 show the longitudinal and transverse sectional plots of HAZ with the optimal combination of scanning velocity and laser beam intensity when $\varphi_{g,\ell}$ increases from 0 to 0.42 ($N = 1$). The complete shrinkage occurs when $\varphi_{g,\ell} = 0.0$ while the HAZ has no shrinkage when $\varphi_{g,\ell} = 0.42$. The partial shrinkage happens as $0.0 \le \varphi_{g,\ell} \le 0.42$. The optimal laser beam intensity increases with increasing $\varphi_{g,\ell}$ because the thickness of the existing sintered layers underneath is higher with higher $\varphi_{g,\ell}$. The shapes of HAZ are similar when the laser scanning speed increases with respect to the specific $\varphi_{g,\ell}$ but the volume of the liquid pool and resolidified region become smaller with increasing laser scanning speed. The overlapped region at the bottom of HAZ of the newly sintered powder layer can be seen and it has reached the bottom of the physical domain. The transverse sections of HAZ are not symmetric along the Y-direction because of the different thermal properties of sintered and unsintered regions.

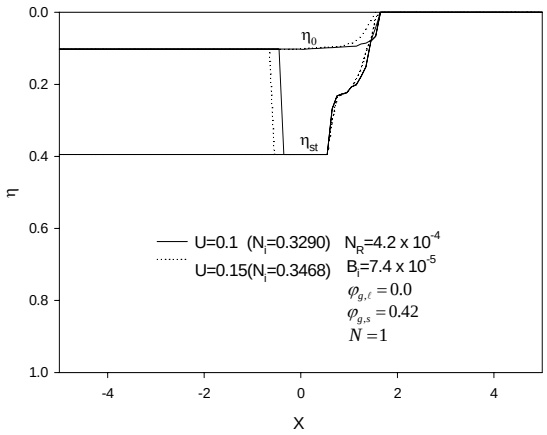


(a)

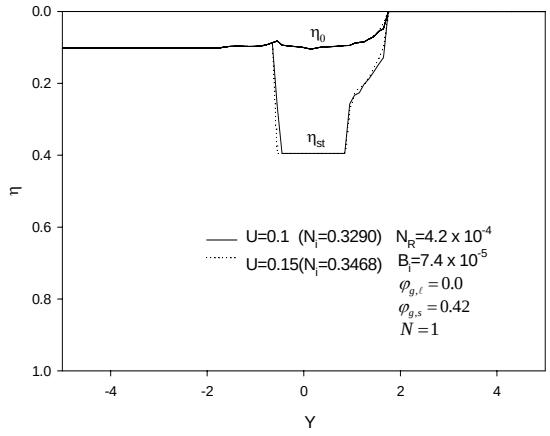


(b)

Fig. 4 Effects of laser intensity and scanning velocity on the sintering process ( $\varphi_{g\ell} = 0.0$ , $N = 1$ )

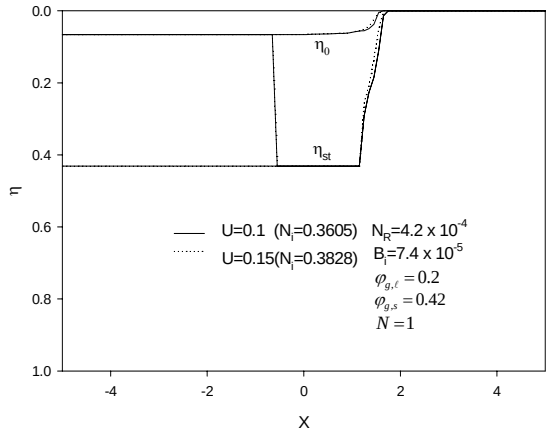


(a)

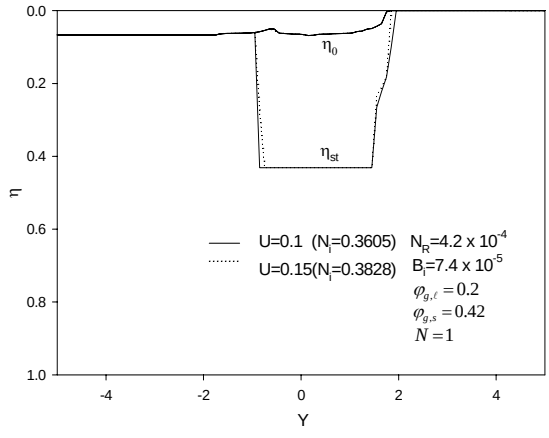


(b)

Fig. 5 Effects of laser intensity and scanning velocity on the sintering process ( $\varphi_{g\ell} = 0.2$ , $N = 1$ )

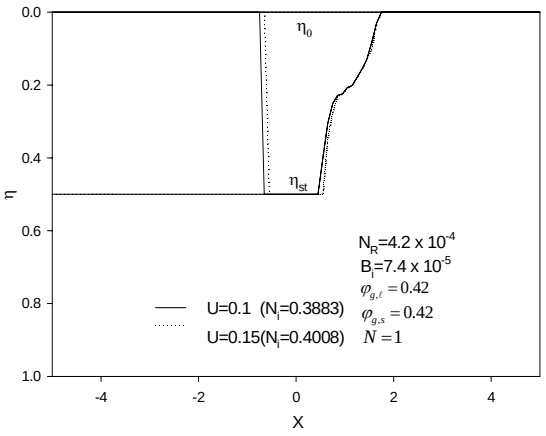


(a)

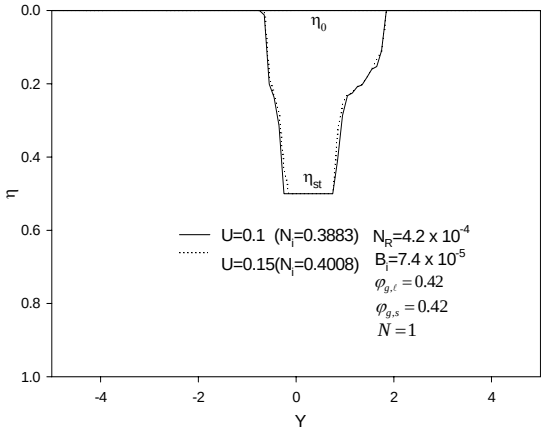


(b)

Fig. 6 Effects of laser intensity and scanning velocity on the sintering process ( $\varphi_{g\ell} = 0.42$ , $N = 1$ )

The optimal combinations of dimensionless scanning velocities and laser beam intensities when $\varphi_{g,\ell}$ increases from 0.0 to 0.42 for $N = 3$ are shown in Figs. 7-9. The laser beam intensity increases significantly with increasing numbers of existing sintered layers underneath with respective to the specific laser scanning velocity. In reality, it is a way to obtain both highly densified sintered part and lower laser beam intensity at the same time by decreasing $\varphi_{g,\ell}$ and then decreasing the thickness of pre-deposited sintered layers below. Accurate density and geometry of the fabricated part are significantly affected by the metallic bonding between layers and the shrinkage. Therefore, the appropriate combination of processing parameters to obtain the desired overlaps and investigation of HAZ formation affected by different shrinkage become necessary.

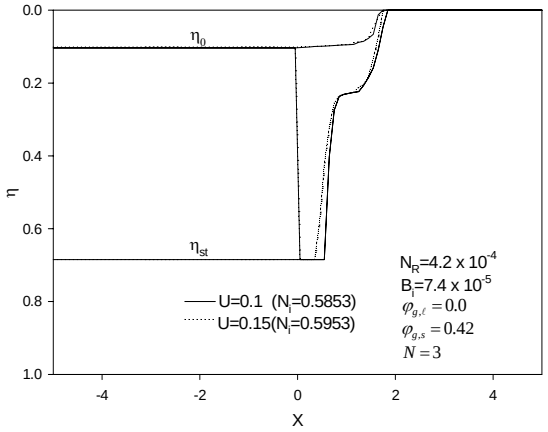


(a)

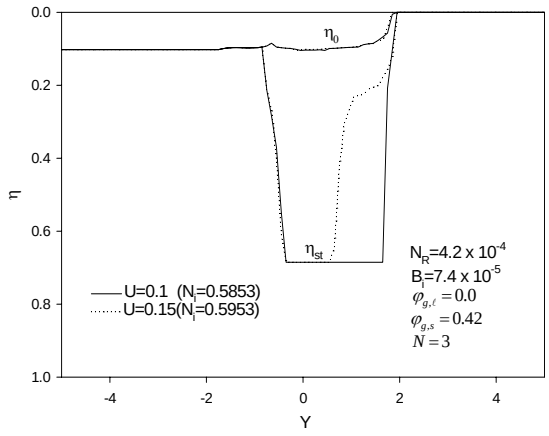


(b)

Fig. 7 Effects of laser intensity and scanning velocity on the sintering process ( $\varphi_{g\ell} = 0.0$ , $N = 3$ )

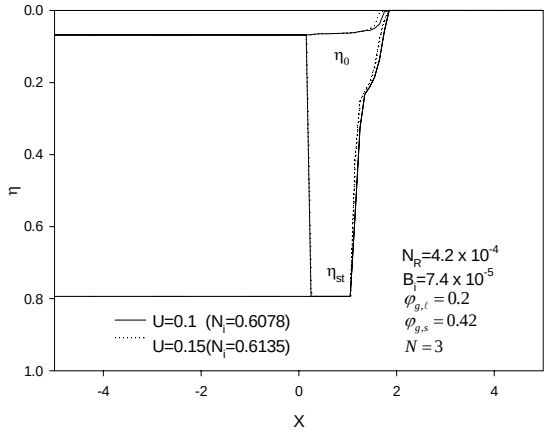


(a)

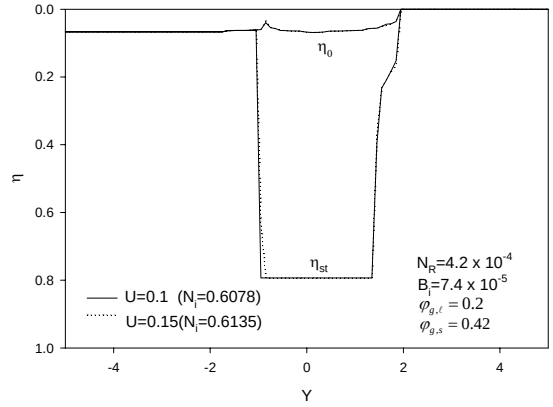


(b)

Fig.8 Effects of laser intensity and scanning velocity on the sintering process ( $\varphi_{g\ell} = 0.2$ , $N = 3$ )

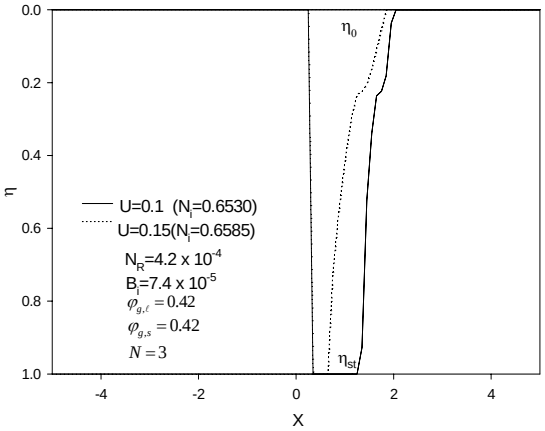


(a)

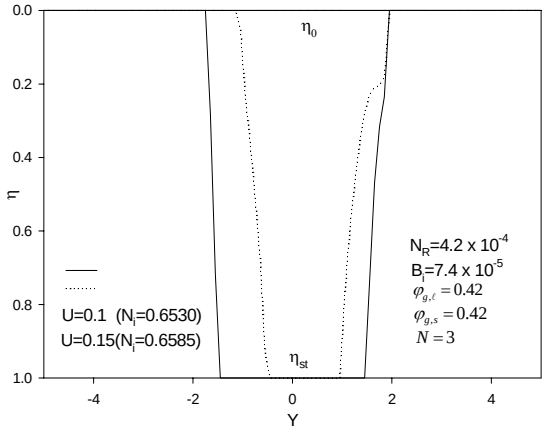


(b)

Fig.9 Effects of laser intensity and scanning velocity on the sintering process ( $\varphi_{g\ell} = 0.42$ , $N = 3$ )

## CONCLUSION

Three-dimensional sintering process of the two-component metal powder layer on top of the existing sintered layers with multiple-line scanning is investigated. The asymmetric geometry in the y-direction due to the overlapped region of neighbored lines considered. The effects of different volume fraction of the gas in HAZ that cause different shrinkage on the sintering process are investigated. The optimal combined dimensionless laser beam intensities and scan velocities are obtained. The results demonstrate that the shape of HAZ significantly affected by the fraction of the gas in HAZ and processing parameters such as the laser beam intensity and the scanning velocity.

## ACKNOWLEDGEMENT

Support for this work by the Office of Naval Research (ONR) under grant number N00014-04-1-0303 is gratefully acknowledged.

## REFERENCE

[1] Conley, J., and Marcus, H., 1997, "Rapid Prototyping and Solid Freeform Fabrication," *Journal of Manufacturing Science and Engineering*, Vol. 119, pp. 811-816.

[2] Agarwala M., Bourell D., Beaman J., Marcus H. and Barlow J., 1995, "Direct Selective Laser Sintering of Metals," *Rapid Prototyping Journal*, Vol. 1, pp. 26-36.

[3] Kumar S., 2003, "Selective Laser Sintering: A Qualitative and Objective Approach," *JOM*, Vol. 55, pp. 43-47.

[4] Viskanta, R., 1983, Phase Change Heat Transfer, in: G.A. Lane (Ed.), *Solar Heat Storage: Latent Heat Materials*, CRC Press, Boca Raton, FL.

[5] Yao, L. C., and Prusa, J., 1989, "Melting and Freezing," *Advances in Heat Transfer*, Vol. 25**,** pp1-96.

[6] Bourell, D.L., Marcus, H.L., Barlow, J.W., and Beaman, J.J., 1992, "Selective Laser Sintering of Metals and Ceramics," *International Journal of Powder Metallurgy*, Vol. 28, No.4, pp. 369-81.

[7] Bunnell, D.E., 1995, *Fundamentals of Selective Laser Sintering of Metals*, Ph.D. Thesis, University of Texas at Austin.

[8] Manzur, T., DeMaria, T., Chen, W., and Roychoudhuri, C., 1996, "Potential Role of High Powder Laser Diode in Manufacturing," presented at SPIE Photonics West Conference, San Jose, CA.

[9] Pak, J., and Plumb, O. A., 1997, "Melting in a Two-Component Packed Bed," *Journal of Heat Transfer*, Vol. 119, pp. 553-559

[10] Zhang, Y., and Faghri, A., 1999, "Melting of a Subcooled Mixed Powder Bed with Constant Heat Flux Heating," *International Journal of Heat and Mass Transfer,* Vol. 42, pp. 775-788.

[11] Chen, T., and Zhang, Y., 2003, "Analysis of Melting in a Mixed Powder Bed with Finite Thickness Subjected to Constant Heat Flux Heating," *Proceeding of ASME Summer Heat Transfer Conference*, Las Vegas, NV.

[12] Zhang, Y., and Faghri, A., 1999, "Melting of a Subcooled Mixed powder Bed with Constant Heat Flux Heating," *International Journal of Heat and Mass Transfer,* Vol. 42, pp. 775-788.

[13] Chen, T., and Zhang, Y., 2004, "Numerical Simulation of Two-Dimensional Melting and Resolidification of a Two-Component Metal Powder Layer in Selective Laser Sintering Process," *Numerical Heat Transfer,* Part A, Vol. 46, No. 7, pp. 633-649.

[14] Kolossov, S., Boillat, E., Glardon, R., Fisher, P., and Locher, M., 2004, "3D FE Simulation for Temperature Evolution in the Selective Laser Sintering Process," *International Journal of Machine Tools and Manufacture*, vol. 44, 117-123.

[15] Zhang, Y., Faghri, A., Buckley, C. W., and Bergman, T. L., 2000, "Three-Dimensional Sintering of Two-Component Metal Powders with Stationary and Moving Laser Beams," *ASME J. Heat Transfer*, Vol. 122, pp. 150-158.

[16] Chen, T., and Zhang, Y., 2005, "Three-Dimensional Modeling of Selective Laser Sintering of Two-Component Metal Powder Layers," *Journal of Manufacturing Science and Engineering*, (Accepted)

[17] Chen, T., and Zhang, Y., 2005, "A Partial Shrinkage Model for Selective Laser Sintering of a Two-Component Metal Powder Layer," *International Journal of Heat and Mass Transfer*, (Accepted)

[18] Chen, T., and Zhang, Y., 2005, "Three-Dimensional Modeling of Laser Sintering of a Two-Component Metal Powder Layer on Top of Sintered Layers," *Proceeding of ASME Summer Heat Transfer Conference*, San Francisco, CA, July 17-22, 2005

[19] Hauser, C., Childs, T. H. C., Dalgarno, K. W., 1999, "Selective Laser Sintering of Stainless Steel 314S HC Processed using room temperature powder beds," *Proceedings of Solid Freeform Fabrication Symposium 1999*, pp. 273-280

[20] Cao, Y. and Faghri, A., 1990, "A Numerical Analysis of Phase Change Problems Including Natural Convection," *Journal of Heat Transfer,* Vol. 112, pp. 812-816.

[21] Kaviany, M., 1995, Principles of Heat Transfer in porous Media, Springer-Verlag, New York.

[22] Patankar, S. V., 1980, *Numerical Heat Transfer and Fluid Flow*, McGraw-Hill, New York.